ChemComm

Boosting mineralized organic pollutants by using sulfur-vacancies CdS photocatalyst

Huijie Wang,[a] Yang Wan,[a] Shikang Yin,[a] Mengyang Xu,[a] Xiaoxue Zhao,[a] Xin Liu,[a] Xianghai Song,[a] Huiqin Wang,[b] Chen Zhu*[c] and Pengwei Huo*[a]

Photocatalytic mineralization of organic pollutions and simultaneously converting CO_2 to CO (tetracycline→CO_2→CO) represents a fascinating way to solve the environmental and energy crisis. This work demonstrates the excellent mineralization and CO_2 reduction performance of S-vacancies CdS and reveals the high efficiency of the carbon self-recycling two-in-one photocatalytic system.

Commonly, CO_2 is one of the final degradation products in the treatment of organic wastewater, which causes a certain waste of carbon resources and is not conducive to improving the increasingly serious greenhouse effect.[1] Given this, a two-in-one system was proposed in a continuous process for photocatalytic oxidation and reduction, which successfully converted the CO_2 to CH_3OH and C_2H_5OH (Table S2).[2] In the system, organic pollutants can be used as hole sacrificial agents, and electrons are employed in the CO_2 reduction process, thus achieving considerable photocatalytic performance. Therefore, using the self-recycling strategy in a two-in-one system to degrade organic pollutants and simultaneously highly selective reduction of the final CO_2 product to CO fuel is an extremely attractive strategy.

CdS photocatalyst typically has a wide visible light absorption range and sufficiently negative potential of the conduction band edge, which is a significant material for the development of photocatalysis technology.[3] Accordingly, the heteroatom doping strategy to metal sulfide proved to be a promising strategy by regulating the energy band position and charge density distribution.[4] In addition, abundant S-vacancies will be obtained in the metal sulfide under the effect of the doped heteroatoms, which will further promote the photocatalytic activity.[5] Notably, Cerium (Ce), with a low redox potential between Ce^{3+} and Ce^{4+}, was usually used to modulate the photocatalytic properties of semiconductor materials.[6] Dai et al. demonstrated that Ce doping-mediated crystal defects not only exerted beneficial effects

on the electron dynamics and energy band structure but also promoted one- and two-electron reactions and significantly enhanced the photoproduction of reactive oxygen species (ROS) by introducing Ce^{3+}/Ce^{4+} redox pairs.[6]

Based on the above consideration, a doping strategy was employed to anchor Ce ions in CdS and create abundant S-vacancies for efficient mineralization of tetracycline (TC) pollutants and reduction of CO_2 to CO in a two-in-one self-recycling photocatalytic system.
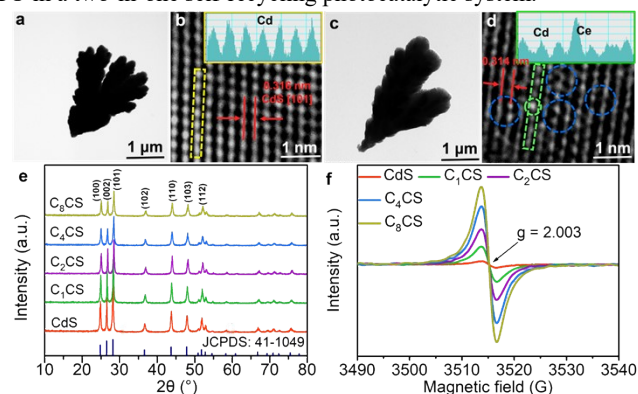

Fig. 1. TEM images of (a) pristine CdS and (c) C_4CS. HRTEM images of (b) pristine CdS and (d) C_4CS (inset figures are the intensity profile of the selected region). (e) XRD spectra and (f) EPR spectra of pristine CdS and C_nCS.

Pristine CdS and Ce-doped CdS (C_nCS) photocatalysts were prepared by a modified hydrothermal method.[7] Transmission electron microscope (TEM) (Fig. 1a and 1c) and the elemental mapping images (Fig. S3b-d, ESI†) of the pristine CdS and C_4CS display that Ce ions evenly deposited in CdS and the morphology was not damaged. The high-resolution transmission electron microscope (HRTEM) observation suggested that the unit cells were arranged regularly with one another, demonstrating good surface crystallinity of the pristine CdS (Fig. 1b). And the interplanar distance is 0.316 nm, corresponding to a lattice spacing of (101) plane for CdS.[8] However, the irregular arrangement and distortion of unit cells and the appearance of vacancies with an interplanar spacing of 0.314 nm are a sign of defective lattice formed by Ce-doped to CdS (Fig. 1d). In addition, the intensity profile atomic dispersion of Ce displayed in Fig. 1d indicated that Ce^{3+}/Ce^{4+} occupies the exact position of the Cd^{2+}.[9]

Powder X-ray diffraction (XRD) patterns were performed to determine the structure information of pristine CdS and C_nCS samples

[a.] Institute of Green Chemistry and Chemical Technology, School of Chemistry & Chemical Engineering, Jiangsu University, Zhenjiang 212013, P. R. China.
[b.] School of Energy and Power Engineering, Jiangsu University, Zhenjiang 212013, P. R. China.
[c.] Department of Molecular and Material Sciences, Graduate School of Engineering Sciences, Kyushu University, Kasuga, Fukuoka 8168580, Japan.

(Fig. 1e). The characteristic peaks of all samples are indexed to hexagonal CdS (JCPDS No. 41-1049).[8] The increased full width at half maximum (FWHM) at 28.2° ((101) planes) of C_4CS compared to that of pristine CdS further illustrated the formation of lattice defects. It is difficult to identify the characteristic peak of Ce in the XRD pattern, which excludes the aggregation of Ce and the presence of new phases. However, the intensity of the peak at 26.5° ((002) plane) of C_nCS samples gradually decreases with the increase of Ce content, which indicates that Ce doping changes the crystal structure of CdS and causes several defects. In addition, there was a peak shift towards the higher degree for the C_nCS with the increase of Ce content compared to pristine CdS for the (002) plane at 26.5°, signifying that the constriction of the crystalline structure, which was also consistent with the HRTEM results for C_4CS. Electron paramagnetic resonance (EPR) and plasma-optical emission spectrometry (ICP-OES) were engaged to evaluate the S-vacancies and concentration of Ce. There just has a weak peak in EPR surveys of pristine CdS, while the gradually strengthened EPR peaks from C_1CS to C_8CS with the g-factor value of 2.003 further indicate that the doping of Ce to CdS has successfully obtained abundant S-vacancies (Fig. 1f).[10] Furthermore, the S-vacancies concentration of pristine CdS and C_nCS (n = 1, 2, 4, 8) detected by EPR were consistent with the results of ICP-OES. (Table S1 and Fig. S1, ESI†). Hence, the results of HRTEM, XRD, EPR and ICP-OES tests fully prove that C_nCS samples have abundant S-vacancies under the effect of Ce doping.
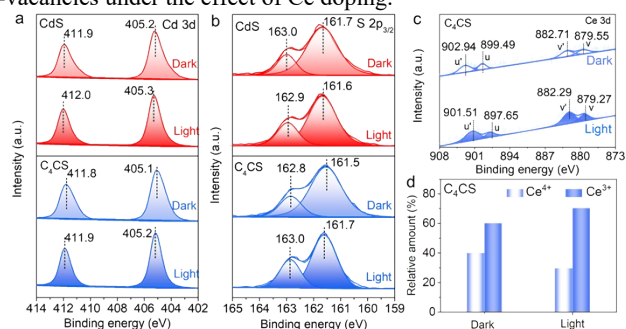

Fig. 2. In-situ XPS spectra of pristine CdS and C_4CS samples tested in darkness and under illumination: (a) Cd 3d, (b) S 2p, and (c) Ce 3d. (d) The relative amount of Ce^{3+} and Ce^{4+} determined through the in-situ XPS spectra of C_4CS under dark and light conditions, respectively.

In-situ XPS was employed to investigate the electron transfer and the state of Ce elements in C_4CS (Fig. 2) under dark and illumination conditions. The high-resolution Cd 3d spectra on pristine CdS and C_4CS had 0.1 eV shifts towards higher binding energy after light illumination compared with a dark condition, which may be due to the transfer of charges around Cd ions to the S site under light conditions (Fig. 2a). The corresponding binding energies in Cd 3d and S 2p spectra of C_4CS shift to lower values in comparison with those of pristine CdS at dark conditions indicating that the large number of S-vacancies created by the doping of Ce affects the Cd-S bond. It was worth pointing out that the two binding energy of Cd 3d and S 2p on C_4CS shift to higher values after illumination relative to dark conditions (Fig. 2a-b). However, all binding energies in the Ce 3d of C_4CS at light conditions exhibit a significant downshift relative to those of dark conditions (Fig. 2c). The XPS spectra confirmed that the charge of pristine CdS shifts to the S sites under light conditions, while the charge shifts around the Ce sites in C_4CS sample.

Additionally, the Ce 3d spectra of C_4CS can be deconvoluted to two peaks of Ce $3d_{3/2}$ and Ce $3d_{5/2}$. The marked peaks at u (899.49 eV) and v (879.55 eV) are attributed to Ce^{4+} $3d_{3/2}$ and Ce^{4+} $3d_{5/2}$, respectively. The peaks labeled as u' (902.94 eV) and v' (882.71 eV) are from the Ce^{3+} species (Fig. 2c).[11, 12] According to the XPS results, the concentration of Ce^{3+} increased from 60 to 70% under the light condition, which proved the reduction of Ce^{4+} to Ce^{3+} (Fig. 2d). Therefore, the increase of charge concentration and the change of the valence state of the Ce^{3+}/Ce^{4+} sites will be helpful to the process of the CO_2 reduction reaction.
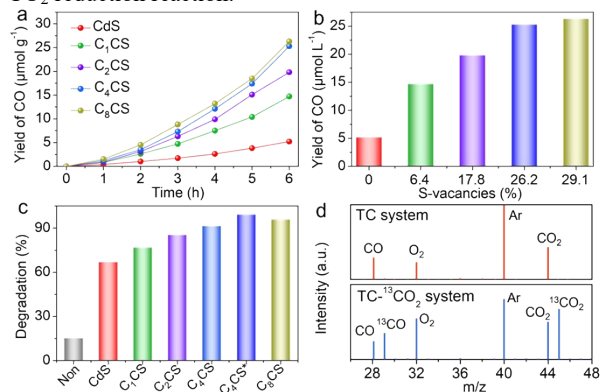

Fig. 3. (a) CO production rates of pristine CdS and C_nCS. (b) The comparison of CO evolution using the pristine CdS and C_nCS with different S-vacancies concentrations. (c) Photocatalytic degradation rates of TC solution over blank, pristine CdS and C_nCS over 6 h (C_4CS* stands for the reaction time was 12 h). (d) Mass spectra of CO (m/z = 28) and ^{13}CO (m/z = 29) production of TC solution system and TC solution-$^{13}CO_2$ system over C_4CS after 2 h photocatalytic reaction under the Ar atmosphere.

The photocatalytic performance of pristine CdS and CnCS samples was tested in a two-in-one system under visible light irradiation, without any sacrificial agent except TC solution (100 mL, 20 mg L^{-1}). The mineralized product of CO_2 and photoreduction product CO as well as the TC degradation rate from the two-in-one system increased as the reaction process continues over pristine CdS and C_nCS catalysts (Fig. 3a, Fig. S4-Fig. S6, ESI†). After a 6 h reaction time, the CO and CO_2 products of pristine CdS were 5.2 and 66.9 μmol g^{-1} (Fig. 3a and Fig. S5a, ESI†), respectively, and the TC degradation rate was 66.9% (Fig. 3c). As expected, the yield of CO and CO_2 as well as the degradation rate of TC have an obvious enhancement with the increase in the amount of Ce, which indicates that S-vacancies and Ce sites can significantly improve the ability to mineralize TC and the CO_2 reduction performance (Fig. 3a-c and Fig. S5a, ESI†). The yield of CO of C_8CS (26.3 μmol g^{-1}) only increased by 4% after 6 h reaction time compared with C_4CS (25.3 μmol g^{-1}), so C_4CS was selected as the model material (Fig. 3a). Control experiment results revealed that the yield of CO and CO_2 products over C_4CS gradually enhances with the increase of TC concentration (Fig. S4 and Fig. S5b, ESI†). It may be that more TC acts as the holes sacrificial agent in the degradation process, which is conducive to more electrons participating in the CO_2 reduction reaction. The yields of CO and CO_2 are increased to 58.1 and 803 μmol g^{-1}, respectively, and the TC degradation rate reached 99.3% after extending the reaction time to 12 h (Fig. 3c and Fig. S6, ESI†). These results also indicate that TC can be fully mineralized to CO_2 under the condition of adequate reaction time and further reduced to CO using the C_4CS photocatalyst. In addition, it is noteworthy that

the CO yield of C_4CS in the two-in-one system was 11.2 times that of the pure CO_2 reduction system (Fig. 3a and Fig. S4, ESI†). $^{13}CO_2$ isotope labeling experiments were performed by gas chromatography-mass spectrometry (GC-MS) to verify the mineralization and reduction ability of C_4CS photocatalyst (Fig. 3d). In a pure TC solution system, the MS signal of photodegradation and photoreduction products at m/z = 44 and 28 are attributed to CO_2 and CO, respectively, which further proves that CO_2 originates from the mineralization of TC solution. The signal at m/z = 29 in the TC solution-$^{13}CO_2$ system further confirms that $^{13}CO_2$ could be converted to ^{13}CO using the C_4CS photocatalyst. It is worth mentioning that the carbon conversion rate of C_4CS reached 1.28% with a 6 h reaction time (Table S1).

The band positions of pristine and C_nCS samples were determined by UV-Vis diffuse reflectance spectra and XPS valence band spectra. A slight red-shift was observed in C_nCS samples compared with pristine CdS, indicating that the light absorption range is not the primary factor to enhance the photocatalytic activity (Fig. S11a, ESI†). In addition, C_4CS has a reduced valence band and a more negative conduction band compared with pristine CdS, suggesting that the introduction of Ce and S-vacancies is accountable for the up-shift of the band position (Table S1, Fig. S11c-d, ESI†).[13] The photocurrent response of transient of pristine CdS and C_nCS samples indicated that the S-vacancies induced by Ce doping can significantly improve the separation of photogenerated electrons and holes (Fig. S12a, ESI†). Electrochemical impedance spectroscopy (EIS) results revealed that the charge transfer resistances of pristine CdS are much higher than that of C_nCS samples (Fig. S12b, ESI†).[14] Additionally, steady-state photoluminescence (PL) spectroscopy of pristine CdS presents a strong emission peak at 428 nm, while the intensity of C_4CS with S-vacancies has an obvious decrease, which demonstrates that the induced S-vacancies by Ce-doping method help to inhibit the recombination of photogenerated carriers (Fig. S12c, ESI†).[15] The time-resolved photoluminescence (TRPL) spectroscopy of pristine CdS and C_4CS results show that pristine CdS has a shorter average lifetime (4.91 ns) than C_4CS (6.97 ns), further confirming that the presence of Ce sites and S-vacancies can enhance the separation efficiency of photogenerated carriers (Fig. S12d, ESI†).

To investigate the mechanism of mineralization and CO_2 reduction, DRIFTS experiments, including the pure CO_2 reduction system (Fig. S13a-b, ESI†) and simulative two-in-one system (Fig. S13c-d, ESI†), were applied over pristine CdS and C_4CS, respectively. Under UV lamp irradiation (420 nm, 3 W, LED), the peaks in the range 2240-2390 cm^{-1} belong to CO_2 adsorbed on the catalyst surface, where the negative peaks at 2268 and 2311 cm^{-1} corresponding to the anti-symmetric stretching vibration of O=C=O of CO_2 (Fig. S13a-b, ESI†). Two broad negative absorption peaks at 3400 and 1650 cm^{-1} emerged and increased in intensity when prolonging irradiation time, which were assigned to the stretching vibration of the O-H bond and the bending vibration of H-O-H of H_2O, respectively (Fig. S13, ESI†). The gradual increase of the negative peak indicates that H_2O participated in the TC photocatalytic degradation and CO_2 reduction process. However, it is interesting to note that the peaks of the C_4CS sample at 3400 and 1640 cm^{-1} in the pure CO_2 reduction system (Fig. S13b, ESI†) and the two-in-one system (Fig. S13d) are much larger than those of the pristine CdS (Fig. S13a and Fig. S13c, ESI†), indicated that the doping effect of Ce and S vacancies can

significantly improve the decomposition of H_2O. The signal at 1620, 1335 and 1165 cm^{-1} are assigned to the intermediate of *COOH, b-CO_3^{2-} and m-CO_3^{-}, respectively, in the CO_2 reduction process. Most importantly, the peak at 2065 cm^{-1} belongs to the CO intermediates (*CO).[16] In addition, there are no obvious CH_4 intermediates (e.g. *CHO and *CHOCO) in situ FTIR, which may be the reason for the high CO selectivity of this work. To further verify that the surface S-vacancies facilitated the promotion of water decomposition, the time profiles on the decay of pristine CdS and C_4CS at 1650 cm^{-1} of the water decomposition signals are shown in Fig. S14 (ESI†). The decay rate constant of C_4CS (-0.0215) is larger than that of pristine CdS (-0.0132), further indicating that S-vacancies can significantly accelerate the decomposition of water, which would decrease the CO_2 reduction reaction energy barrier according to our previous study.[13]
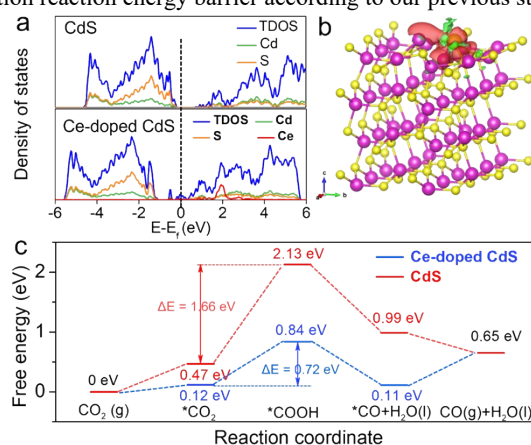

Fig. 4. (a) The DOS of pristine CdS and Ce-doped CdS (the dashed line represents the Fermi level). (b) The charge density difference of Ce-doped CdS (Red electron cloud represents the accumulation of electrons; Green electron cloud represents electron consumption). (c) Gibbs free energy diagrams of the photocatalytic CO_2 reduction process for pristine CdS and Ce-doped CdS.

The density functional theory (DFT) calculations were applied to investigate the charge transfer mechanism affected by the Ce sites on the surface of Ce-doped CdS and the effect of S-vacancies on the CO_2 reduction reaction. The density of states (DOS) revealed that the Ce-doped CdS with S-vacancies obtained a new state near the Fermi level, indicating that the photogenerated charge transfer capability was enhanced and facilitated the reduction of CO_2 (Fig. 4a). The C atom in the CO_2 molecule has low electronegativity. In theory, the captured electrons at the Ce^{3+}/Ce^{4+} sites can be transferred to the C atom from the surface-adsorbed CO_2 molecule. Therefore, the Ce^{3+}/Ce^{4+} site could act as an alternative reactive site for promoting the activation of the C=O bond and CO_2 reduction reactions. The charge density difference of Ce-doped CdS exhibits that electron enrichment occurs around the Ce atom, which proves that the Ce site plays a role in electron capture, which will contribute to the reduction of CO_2 (Fig. 4b).[17] It can be seen from the charge density distribution diagram that the charge density of the Cd-S bond in Ce-doped CdS is significantly weaker than that of pristine CdS. However, Ce sites have a strong charge density, indicating that a large number of electrons will be transferred to Ce sites, which is consistent with the results of in-situ XPS (Fig. S18, ESI†). The C=O band length of the CO_2 molecules (1.176 Å) had a significant change (1.184/1.168 Å) during the process of charge transfer from Ce sites to CO_2, which revealed that Ce site as the charge trapping center contributes to the polarization of CO_2

molecules (Fig. S19, ESI†). Moreover, on the surface of pristine CdS, the reaction energy barrier (ΔE) for CO_2 adsorption and activation to *CO_2 is 0.47 eV, which is much higher than that on the surface of Ce-doped CdS (0.12 eV) with S-vacancies (Fig. 4c). The ΔE of *CO_2 further converted to *COOH was 1.66 eV over pristine CdS in the photocatalytic reduction process involving water molecules. However, the transformation from *CO_2 to *COOH decreased to 0.72 eV on the surface of Ce-doped CdS, indicating that S-vacancies contribute to a decrease in the reaction activation energy for CO_2 reduction, and this result is also consistent with our previous findings. The further reduction of *COOH to *CO decreases from 0.99 to 0.11 eV, indicating that CO can be obtained more easily on the surface of Ce-doped CdS, which completely coincides with the experimental and photoelectrochemical measurements.[18] Therefore, it is reasonable to speculate that the S-vacancies induced by Ce doping reduce the reaction activation energy and the enhanced charge density of Ce sites increasing the separation and transfer capability of charge carriers, thus enhancing the CO_2 photoreduction activity.

In summary, we report an efficient and stable S-vacancies CdS material induced by the Ce-doping strategy for photocatalytic mineralization of organic pollutants and the photoreduction of CO_2 through carbon self-recycling for CO production. The DFT calculation and experimental results indicate that S-vacancies decreased the reaction activation energy of CO_2 reduction, and the enhanced charge density around the anchored Ce ions acting as reactive sites promote charge separation and transfer. As a consequence, the photoreduction activity of the C_4CS sample increased by 5 times compared to pristine CdS in the two-in-one system. In addition, the CO yield in the two-in-one system was 11.2 times that in a single CO_2 reduction system. This work utilizes a two-in-one self-recycling system to efficiently mineralize organic pollutants and selectively produce CO, which provides a certain reference for the study of efficient degradation of organic pollutants and CO_2 reduction.

Conflicts of interest
There are no conflicts to declare.

Notes and references
1   Y. Cui, Y. Li, Y. Liu, D. Shang, Y. Liu, L. Xie, S. Zhan and W. Hu, *Chem. Commun.*, 2022, **58**, 4251-4254.
2   J. Zou, D. Wu, J. Luo, Q. Xing, X. Luo, W. Dong, S. Luo, H. Du and S. L. Suib, *ACS Catal.*, 2016, **6**, 6861-6867.
3   P. Xia, X. Pan, S. Jiang, J. Yu, B. He, P. M. Ismail, W. Bai, J. Yang, L. Yang, H. Zhang, M. Cheng, H. Li, Q. Zhang, C. Xiao and Y. Xie, *Adv. Mater.*, 2022, **34**, e2200563.
4   H. Cao, J. Xue, Z. Wang, J. Dong, W. Li, R. Wang, S. Sun, C. Gao, Y. Tan, X. Zhu and J. Bao, *J. Mater. Chem. A*, 2021, **9**, 16339-16344.
5   J. Yuan, X. Yi, Y. Tang, M. Liu and C. Liu, *Adv. Funct. Mater.*, 2019, **30**, 1906983.
6.   Z. Dai, F. Qin, H. Zhao, J. Ding, Y. Liu and R. Chen, *ACS Catal.*, 2016, **6**, 3180-3192.
7   N. Lakshmana Reddy, V. N. Rao, M. M. Kumari, P. Ravi, M. Sathish and M. V. Shankar, *Mater. Res. Bull.*, 2018, **101**, 223-231.
8   D. Zhang, J. Teng, H. Yang, Z. Fang, K. Song, L. Wang, H. Hou, X. Lu, C. R. Bowen and W. Yang, *Carbon Energy*, 2022, **277**, 1-14.
9   J. Zhang, X. Xu, L. Yang, D. Cheng and D. Cao, *Small Methods*, 2019, **3**, 1900653.
10   Y. Tan, Z. Chai, B. Wang, S. Tian, X. Deng, Z. Bai, L. Chen, S. Shen, J. Guo, M. Cai, C. Au and S. Yin, *ACS Catal.*, 2021, **11**, 2492-2503.
11   J. Liu, Y. Liu, X. Mu, H. Jang, Z. Lei, S. Jiao, P. Yan, M. G. Kim and R. Cao, *Adv. Funct. Mater.*, 2022, **32**, 2204086.
12   J. Li, S. Zou, X. Liu, Y. Lu and D. Dong, *ACS Sustainable Chem. Eng.*, 2020, **8**, 10009-10016.
13   S. Yin, X. Zhao, E. Jiang, Y. Yan, P. Zhou and P. Huo, *Energy Environ. Sci.*, 2022, **15**, 1556-1562.
14   M. Yuan, J. Chen, Y. Bai, Z. Liu, J. Zhang, T. Zhao, Q. Wang, S. Li, H. He and G. Zhang, *Angew. Chem. Int. Ed. Engl.*, 2021, **60**, 10910-10918.
15   F. Chen, Y. Li, M. Zhou, X. Gong, Y. Gao, G. Cheng, S. Ren and D. Han, *Appl. Catal., B*, 2023, **328**, 122517.
16   J. Li, H. Huang, W. Xue, K. Sun, X. Song, C. Wu, L. Nie, Y. Li, C. Liu, Y. Pan, H. Jiang, D. Mei and C. Zhong, *Nat. Catal.*, 2021, **4**, 719-729.
17   G. Wang, Y. Wu, Z. Li, Z. Lou, Q. Chen, Y. Li, D. Wang and J. Mao, *Angew. Chem. Int. Ed. Engl.*, 2023, e202218460.
18   N. Li, X. Chen, J. Wang, X. Liang, L. Ma, X. Jing, D. L. Chen and Z. Li, *ACS Nano*, 2022, **16**, 3332-3340.